



Cite this: *Dalton Trans.*, 2024, **53**, 14496

## Structural diversity and solvent-induced transformations of a copper-based metal–organic framework with highly aromatic ligands<sup>†</sup>

Abigail Edwards,<sup>a</sup> Landon J. Elkins,<sup>a</sup> Carla Slobodnick,<sup>ID</sup><sup>b</sup> Jinglei Wang,<sup>c</sup> Qiang Zhang<sup>ID</sup><sup>c</sup> and Tegan A. Makal<sup>ID</sup><sup>\*</sup><sup>a</sup>

A newly designed tetracarboxylic acid ligand precursor 5,5'-(9,9'-bianthracene)-10,10'-diyl)diisophthalic acid (H<sub>4</sub>BADI) has been used to prepare a series of copper-based metal–organic frameworks (MOFs) with the formula [Cu<sub>2</sub>(BADI)(S)<sub>2</sub>]<sub>x</sub>S (denoted as **1**–S, where S = solvent) and exhibiting solvent-induced structural transformations. Single-crystal-to-single-crystal transformation occurs upon exchanging **1**–DMF (DMF = *N,N*-dimethylformamide) with DMSO (DMSO = dimethylsulfoxide). **1**–DMF exhibits reversible structural transformation upon treatment with a variety of solvents; of particular interest is the reversible crystalline-to-amorphous phase transformations observed upon exchange with volatile, polar solvents. A thorough structural investigation of the three framework isomers characterized via single-crystal X-ray diffraction experiments is reported and compared to several other tetracarboxylate-based MOFs composed of dimetal secondary building units.

Received 19th July 2024,  
Accepted 3rd August 2024  
DOI: 10.1039/d4dt02085e  
[rsc.li/dalton](http://rsc.li/dalton)

## Introduction

Metal–organic frameworks (MOFs) are coordination networks with metal nodes and organic ligands containing potential voids,<sup>1</sup> and have garnered significant interest owing to their structural diversity, tunability, and potential for application in a variety of industries.<sup>2–4</sup> Among porous materials, MOFs are unique in that many exhibit structural flexibility upon external stimuli (solvent/guest species, pressure, and temperature) as a result of being composed of strong but flexible coordination bonds and/or organic covalent bonds.<sup>5,6</sup> An excellent review article examining the features of MOF flexibility and providing greater analysis of different types of flexibility has been published recently.<sup>7</sup> In the area of stimuli-responsive MOFs, single-crystal-to-single-crystal (SCSC) transformations typically generate the highest level of interest.<sup>8</sup> However, while the majority of reports involving flexibility in MOFs have focused

on crystalline phase transformations, the formation of amorphous MOFs with minimal loss in structural integrity has garnered rising attention. Limited reports exist evaluating such transformations, though Pallach *et al.* coined the term “frustrated flexibility in MOFs” to describe the process by which MOFs may undergo amorphization while maintaining framework connectivity due to “an incompatibility of intra-framework dispersion forces with the geometrical constraints of the inorganic building units”.<sup>9</sup> This frustrated flexibility can occur in seemingly rigid MOFs and results in reversible loss and recovery of crystalline order. The study of flexibility in MOFs provides significant insights into structure–property relationships and can lead to the realization of gated guest-uptake mechanisms, a feature highly sought after for the development of materials for selective adsorption and gas storage and delivery.<sup>5</sup>

We have been particularly interested in the development of MOFs with highly aromatic ligands due to previous theoretical studies indicating that incorporation of highly aromatic groups could lead to enhanced functional properties,<sup>10</sup> however, only a few such MOFs have been reported, likely due to perceptions of the organic ligands being synthetically challenging to isolate and exhibiting poor solubilities. ZJU-105, a copper-based MOF (CuMOF) incorporating a tetracarboxylate binaphthalene moiety, has been reported.<sup>11</sup> The compound, which is a top performer in methane delivery capacity, has a structure that is comparable to those of other CuMOFs with rectangular planar tetracarboxylate ligands.<sup>11</sup> The well-known

<sup>a</sup>Department of Natural Sciences, The University of Virginia's College at Wise, 1 College Avenue, Wise, VA 24293, USA. E-mail: tam9k@uvawise.edu

<sup>b</sup>Department of Chemistry, Virginia Tech, Blacksburg, Virginia 24060, USA

<sup>c</sup>Department of Chemistry, Washington State University, Pullman, Washington 99164, USA

<sup>†</sup>Electronic supplementary information (ESI) available: Ligand synthesis; <sup>1</sup>H, <sup>13</sup>C, <sup>1</sup>H–<sup>1</sup>H COSY, <sup>1</sup>H–<sup>13</sup>C HSQC, and <sup>1</sup>H–<sup>13</sup>C HMBC NMR spectra; overview of MOF synthesis; single-crystal X-ray diffraction experimental; MOF structures; PXRD patterns; TGA data; gas adsorption isotherms; and IR spectra. CCDC 2324983–2324986 and 2371664. For ESI and crystallographic data in CIF or other electronic format see DOI: <https://doi.org/10.1039/d4dt02085e>



cage-like structure of ZJU-105 (present in materials such as the NOTT-10X series,<sup>12</sup> PCN-14,<sup>13</sup> and Cu<sub>2</sub>ADEDA<sup>14</sup>) lends itself to inherent porosity and stability that is highly desirable in MOF design. Taking inspiration from ZJU-105 and PCN-14, we synthesized the novel, highly aromatic ligand precursor H<sub>4</sub>BADI (5,5'-(9,9'-bianthracene]-10,10'-diyl)diisophthalic acid) to investigate the potential of a bianthracene moiety in the formation of Cu and Zn MOFs.

Herein, we report the synthesis and characterization of a related series of CuMOFs with BADI as the organic linker. These CuMOFs exhibit solvent-induced structural transformations. We also present a ZnMOF with a structure very different from the CuMOFs that suggests that Zn, in this situation, is much less interesting with regard to potential real-world applications. Characterization methods include powder X-ray diffraction (PXRD), thermogravimetric analysis (TGA), and IR-spectroscopy. Additionally, three forms of the CuMOFs and the ZnMOF have been characterized by single-crystal X-ray diffraction.

## Results and discussion

### Synthesis

1-DMA, 1-DMF, and 1-DEF are isolable as green crystalline solids (Fig. S19†) under solvothermal reaction conditions between Cu(NO<sub>3</sub>)<sub>2</sub>·2.5 H<sub>2</sub>O and H<sub>4</sub>BADI in DMA, DMF, and DEF, respectively, with varying amounts of HBF<sub>4</sub> and heating at 85 °C in an oven for 2 days (Fig. 1). In general, crystallite sizes increased with increasing the amount of HBF<sub>4</sub> in the reaction mixture. [Note: No attempts were made to prepare 1-S

with a lower volumetric ratio than 7.5 solvent per 1 HBF<sub>4</sub>.] Depending on exact reaction conditions and reaction time, Cu(0) was often observed alongside crystalline 1-S. Generally, longer reaction times (>2 days) and higher concentrations of HBF<sub>4</sub> resulted in increased production of Cu(0). Details regarding the handling of Cu(0) are provided in the ESI.† For all reported MOFs, the crystalline solid was obtained by decanting the mother liquor, washing with fresh synthesis solvent, and allowing the solid to dry under ambient laboratory conditions on filter paper. Individual crystals for single-crystal X-ray diffraction measurements were removed directly from the mother liquor or from suspension in fresh solvent. Bulk phase purity was evaluated by PXRD measurements and compared to patterns simulated from single-crystal XRD data (Fig. 2a).

Intrigued by the isolation of 1-S framework isomers from different solvents, we investigated the preparation of 1 in mixed solvent systems. A range of solvent ratios from 10 : 1 to 1 : 1 (DMA : DMF, v : v) were tested, with 5 : 1 and larger ratios giving 1-DMF, ratios of 3 : 1 and 4 : 1 DMF : DMA giving a mixture of 1-DMA and 1-DMF phases, and 2 : 1 and lower ratios giving 1-DMA, exclusively (Fig. 2b).

We also explored the preparation of the CuMOF, ZJU-105 (ligand = 5,5'-(1,1'-binaphthalene)-4,4'-diyl)diisophthalic acid, H<sub>4</sub>BNDI) under a variety of solvothermal reactions, including DMA or DMF as solvent. We highlight two notable conditions in the ESI,† as we successfully isolated exceptional quality single crystals of ZJU-105 exhibiting distinct edges and the typical crystal shape of **nbo**-type (**fof**-type) MOFs belonging to the *R*3*m* space group as compared to the previous report<sup>11</sup> (Fig. S18†). Bulk ZJU-105 powder (which is generally more easily formed into monoliths or shaped samples) was also isolable with stirring in an oil bath (ZJU-105(stirred)).

### Structural descriptions

1-DMA crystallizes in the monoclinic space group *P*2<sub>1</sub>/*n* (#14, lattice parameters: *a* = 10.71 Å, *b* = 37.18 Å, *c* = 14.77 Å,  $\beta$  = 92.98°). The asymmetric unit of 1-DMA consists of two Cu(II) ions, one BADI<sup>4-</sup> ligand, and two DMA molecules coordinated to the terminal positions of the dicopper-paddlewheel. During preliminary refinements, there was evidence of three disordered DMA molecules in the asymmetric unit, but efforts to model the disorder were unsuccessful, presumably due to significant positional and/or dynamic disorder within the structural cavities. These solvent molecules were masked out in the final structural model.

For 1-DMF, initial assessment of both PXRD and single-crystal XRD data led to assignment to the orthorhombic space group *C*ccm (*a* = 11.35 Å, *b* = 36.37 Å, *c* = 14.78 Å). However, in this space group, there were systematically weak non-indexed reflections in the single-crystal XRD data, suggesting a superlattice, and the preliminary structural model showed significant BADI<sup>4-</sup> ligand disorder with unreasonable steric interactions. Upon more careful analysis of the diffraction data, a monoclinic nonmerohedral twin was identified (twin law 180° rotation about [001]) that accounted for the majority of the systematically weak reflection. Following this analysis, 1-DMF was

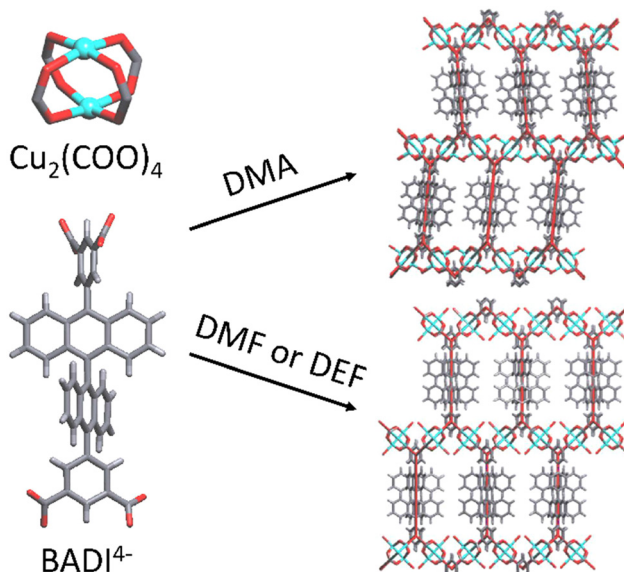
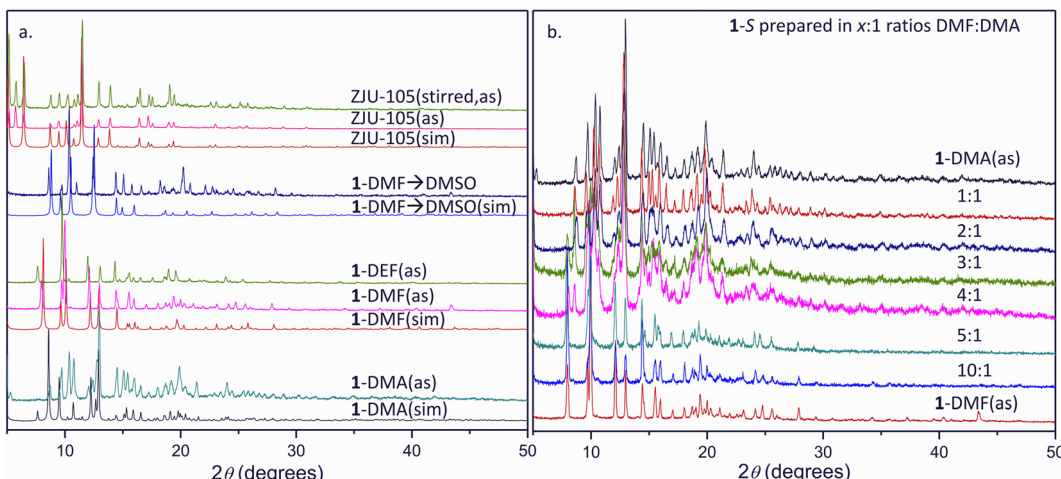


Fig. 1 Secondary building units in the formation of 1-S and schematic structure overlaid underlying net topology. Oxygen = red; copper = teal; carbon = dark gray; and hydrogen = light gray. Underlying net topology (generated by treating Cu<sub>2</sub>(COO)<sub>4</sub> as a 4-connected node and BADI as two 3-connected nodes) represented by teal and red sticks, respectively.





**Fig. 2** Experimental PXRD patterns of (a) **1-S** and ZJU-105 versus simulated patterns from single-crystal structures (sim), and (b) **1-S** prepared with varying ratios of DMF : DMA. “as” = as-synthesized and “DMF → DMSO” = **1-DMF** soaked in DMSO for 18 h at 85 °C.

identified to crystallize in the monoclinic space group *P*2/c (#13, lattice parameters:  $a = 19.19$  Å,  $b = 14.79$  Å,  $c = 22.90$  Å,  $\beta = 107.26^\circ$ ). The asymmetric unit of **1-DMF** is composed of two Cu(II) ions, one BADI<sup>4-</sup> ligand, and two solvent molecules (modeled as water, but likely a combination of water and DMF) coordinated to the terminal positions of the dicopper-paddlewheel. During structural refinement on the HKLF 5 twin data, the twin ratios were refined to approximately 50/50 (0.516(2) and 0.484(2)) accounting for the pseudo-orthorhombic symmetry.

Single-crystal XRD analysis of **1-DEF** led to the initial determination of cell parameters comparable to those of **1-DMF**. Refinement of the structural model was unsuccessful, however, owing to significant disorder within the system. Based on cell parameters and comparable PXRD patterns, **1-DEF** is determined to be isostructural with **1-DMF**.

Single crystals of **1-DMSO** were isolated from a DMSO-exchanged sample of **1-DMF**, and solved and refined in the orthorhombic space group *Cccm* (#66, lattice parameters:  $a = 10.41$  Å,  $b = 36.76$  Å,  $c = 15.48$  Å) to give a model that is isostructural with the **1-DMF** model when it was refined in *Cccm*. While the crystal likely has the same nonmerohedral twinning issues as **1-DMF**, the solvent exchange caused an overall degradation in crystal (and data) quality, and we were unable to obtain usable HKLF 5 data to refine as the ordered twinned model in space group *P*2/c. In the structural model from the twinned orthorhombic cell, the asymmetric unit consists of one-half of a Cu(II) ion, one-quarter of a BADI<sup>4-</sup> ligand, and one-half of a solvent molecule (modeled as water) coordinated to the terminal position of the dicopper-paddlewheel.

The three distinct phases of **1-S** are constructed from dicopper(II)-paddlewheel SBUs and BADI<sup>4-</sup> ligands in a 1 : 1 stoichiometric ratio (Fig. 3), with solvent molecules (water and/or DMA/DMF/DMSO) occupying terminal coordination sites on the metal SBU as well as within the pores of the structure. The frameworks of **1-DMA**, **-DMF**, and **-DMSO** may be described as

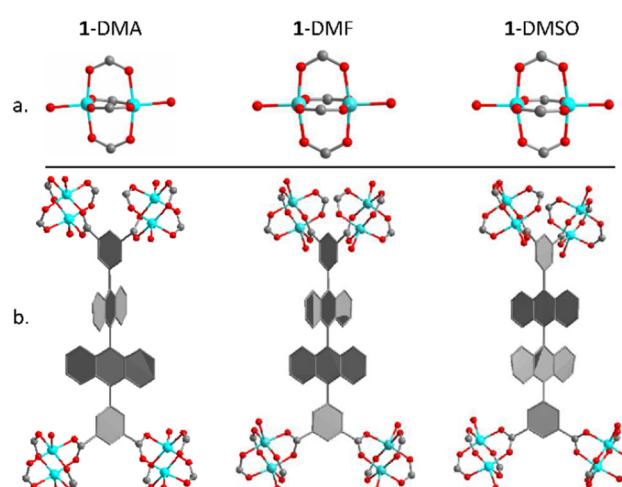


**Fig. 3** (a) Dicopper paddlewheel and (b) ligand SBUs found in **1-DMA**, **-DMF**, and **-DMSO**. Oxygen = red; copper = teal; and carbon = gray. Solvent molecules found in the terminal positions of paddlewheels are truncated at the oxygen. Hydrogen atoms are not shown for structural clarity.

2-D sheets constructed from isophthalate-bridged dicopper paddlewheels extended into the third dimension through the bianthracene moiety (Fig. 4, S20 and S21†), comparable to what has been reported for NOTT-109.<sup>12</sup>

In **1-DMA**, the metal-isophthalate layers span the *ac*-plane with bianthracene extending along the *b*-direction to produce a 3-D MOF. The bianthracene moieties deviate from being parallel to the *b*-axis by approximately 5°, resulting in organic layers alternating the direction of tilt, owing to the  $2_1$ -screw axis (Fig. 4). When viewed downwards (100), zig-zag channels appear to be present running parallel to the *c*-axis but are highly congested due to the bulky anthracene groups (Fig. S21 and S22†). The zig-zag channels may be considered as



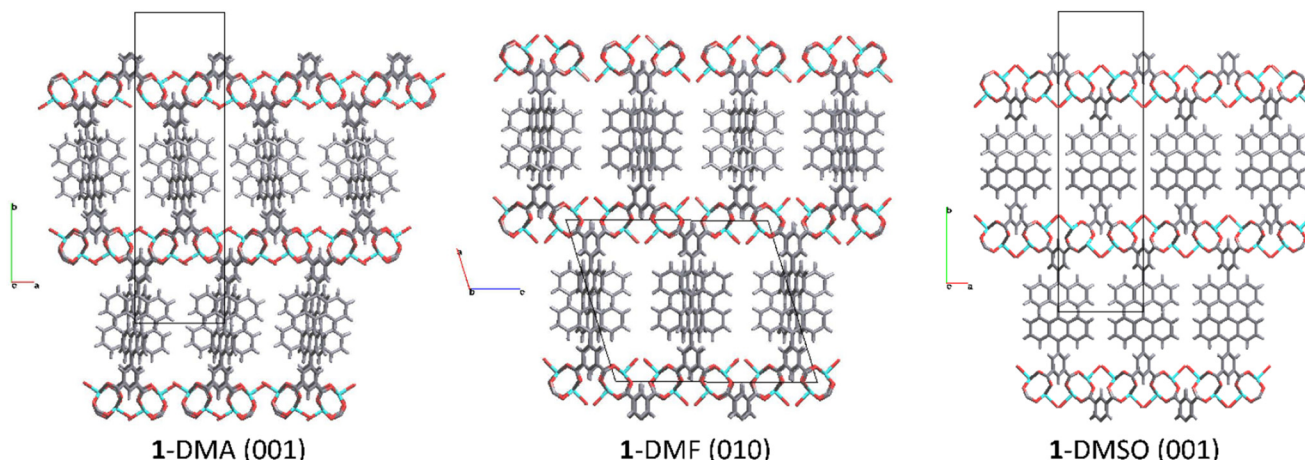


**Fig. 4** Crystal packing in **1-S** highlighting extension of metal–isophthalate layers by the bianthracenyl moiety. The viewing direction for each structure is indicated following the structure name as the direction normal to  $(hkl)$ . Oxygen = red; copper = teal; carbon = dark gray; and hydrogen light gray.

irregular-shaped (pseudo-rectangular prismatic) “cages” propagating along the  $c$ -axis. The “cages” form between bianthracene “walls” and are capped by the metal–isophthalate layers, with pore sizes of approximately  $5\text{ \AA} \times 5\text{ \AA} \times 13\text{ \AA}$  (Fig. 5).

In **1-DMF**, the Cu-isophthalate layers span the  $bc$ -plane and extend parallel to the  $a^*$ -direction *via* bianthracene moieties to form a 3-D MOF. Unlike in **1-DMA**, the bianthracene units in **1-DMF** are arranged parallel to one another and almost perfectly parallel to the  $a^*$  axis (Fig. 4). While the pore structure of **1-DMF** is similar to that of **1-DMA** (Fig. 5), the orientation of anthracene groups results in enhanced solvent-accessible voids (20.2% *vs.* 12.3%, respectively, when calculated using a spherical probe radius of  $1.2\text{ \AA}$ , Fig. S22†).

Similar to **1-DMA**, **1-DMSO** may also be described by Cu-isophthalate layers spanning the  $ac$ -plane, with bianthracene groups extending the structure along the  $b$ -direction. However, in this twinned orthorhombic  $Cccm$  structural model, the disordered ligands must align perfectly parallel to the  $b$ -axis by

symmetry. The pore structure of **1-DMSO** is comparable to those of **1-DMA** and **1-DMF**.

A key feature of the three **1-S** structures is the significant distortions from planarity between carboxylates and the attached phenyl rings. For an isolated isophthalate group, the minimum overall energy is achieved when all the atoms of the functional group are coplanar, resulting in greater delocalization of the electron density throughout the  $\pi$ -aromatic system. Of course, many factors play roles in the MOF self-assembly process, in which balances are made between different sources of strain in order to minimize the total energy of the crystalline system. The dihedral angles between planes formed by each carboxylate and isophthalate phenyl group (*e.g.*, Fig. 6,  $\angle C1 P1$ ), as well as isophthalate–isophthalate (*e.g.*, Fig. 6,  $\angle P1 P3$ ) and carboxylate–carboxylate angles (*e.g.*, Fig. 6,  $\angle C1 C2$ ,  $\angle C1 C3$ ), were measured using Mercury and are reported in Table S3.†<sup>15</sup> These measurements are used to highlight the significant variations from other dicopper-tetracarboxylate MOFs.

Dicopper-paddlewheel/tetracarboxylate **nbo**-type MOFs require (near) coplanarity of all four carboxylate groups to produce their characteristic hierarchical, cage-like structures.

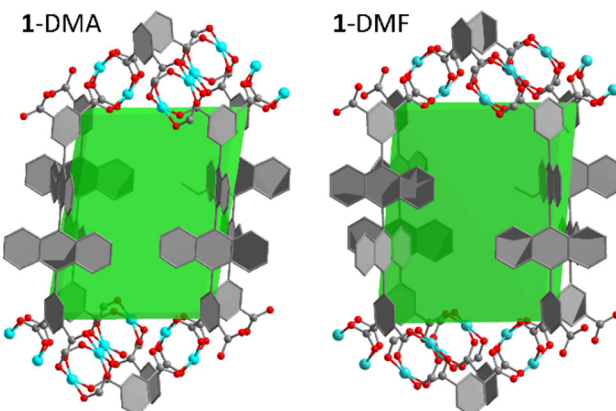


**Fig. 5** Cage-like pores in **1-S** generated from four adjacent bianthracenyl groups bridging metal–isophthalate layers. **1-DMA** is viewed along [001] and **1-DMF** is viewed along [010].

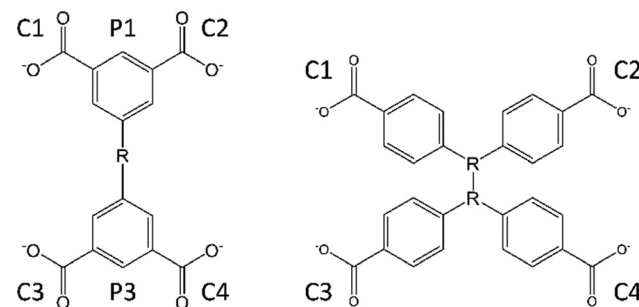


**Fig. 6** Labeling system used for identifying dihedral angles between planes prepared from O–C–O atoms in carboxylates (C1–C4) and carbon atoms in phenyl rings (P1 and P3) in diisophthalate (left) and tetrabenzoate (right) ligands.

For instance,  $\angle P1\ P3$  in representative examples of **nbo**-type MOFs (ZJU-105,<sup>11</sup> NOTT-102,<sup>12</sup> PCN-14,<sup>13</sup> and Cu<sub>2</sub>ADEDA<sup>14</sup>) are all 0°. Furthermore, the largest difference in angle between planes generated by carboxylates in these MOFs is 12°, observed in PCN-14 (which consists of sterically bulky anthracene moiety directly bound to both isophthalate groups). By comparison, NOTT-109,<sup>12</sup> which adopts an **ssb**-type structure, replaces the anthracene in PCN-14 with a naphthalene moiety and exhibits substantial out-of-the-plane “flexing” in the ligand in its formation of cage-like pores. As an example, the isophthalate-isophthalate phenyl angle is 18° and the deviations between carboxylate planes are as large as 52°.

Isophthalate-isophthalate phenyl angles in **1-S** range between ~70 and 80°. Additionally, the angles between carboxylates and the attached phenyl rings are all around 30°, a significant deviation from the preferred near-coplanar conformation. Since **1-DMSO** was unable to be fully refined as ordered in the monoclinic *P2/c* space group, **1-DMF** was also refined as disordered in the higher symmetry *Cccm* space group generated by the peak overlap in the 50/50 non-merohedral twin. This allows for a direct comparison between the two structures. Notably, in comparing the structural models of **1-DMF** in *P2/c* vs. *Cccm*, no measured dihedral angle differed by more than 5°, indicating that reliable interpretations of structural features may be obtained from the structural model, providing confidence in the evaluation of our twinned/disordered *Cccm* model for **1-DMSO**.

Comparing the structural models for **1-DMA** (*P2<sub>1</sub>/n*), -DMF (both *P2/c* and *Cccm*), and -DMSO (*Cccm*), the difference in individual dihedral angles across the structural models differed by as much as 12° (Table S3†). The isophthalate-isophthalate phenyl angles ( $\angle P1\ P3$ ) in **1-DMF** and -DMA differ by only 2°, while **1-DMSO** differs from -DMF and -DMA by 12 and 10°, respectively. Carboxylate-carboxylate angles show greater variability between models, with a maximum deviation of 12° in  $\angle C1\ C4$  between **1-DMA** and **1-DMSO**. These variances in unit cell parameters and symmetries highlight the impacts of introducing different solvents into the MOF system, and how metal- and organic-SBUs may be affected by external stimuli. In particular, the primary factor impacting the phase that forms for **1-S** is presumed to be the terminally coordinated solvent molecules. The acetyl groups of DMA on neighboring dicopper-paddlewheel SBUs orient toward one another, resulting in distortions to the paddlewheel, whereas formyl groups of DMF and DEF permit terminal copper positions to lie nearer each other, thereby alleviating some of the angle strain. Though coordinated solvent molecules could not be located in the structure of **1-DMSO**, based on similarities to the -DMF structure and lack of significant distortions in the metal SBU, we can infer that DMSO contributes to steric repulsions more akin to DMF than DMA. In evaluating the Cu–Cu distances between nearest neighboring SBUs, we find that the shortest distances in **1-DMF** and -DMSO are 8.308 and 8.425 Å, respectively, whereas the same measurement in **1-DMA** is ~0.5 Å shorter (7.817 Å, Fig. S20†). We explore the impacts of solvent further in the next section regarding solvent-induced phase transformations.

One method to enhance the potential to produce coplanar carboxylates is to use an odd number of phenyl-spacers between isophthalate groups. Since biphenyl-like systems generally lie out of plane with one another to reduce steric repulsions between C–H groups, ligands with an even number of phenyl spacers between isophthalates provide an increased barrier to the production of coplanar carboxylates. The cage-like structures of **nbo**-type MOFs can overcome some steric repulsions, as observed in NOTT-102<sup>12</sup> and ZJU-105;<sup>11</sup> however, the repulsions experienced between C(1)–H and C(8)–H groups of adjacent anthracenyl moieties in BADI<sup>4-</sup>, as well as repulsions of C(4)–H and C(5)–H groups of anthracene with C(4)–H and C(6)–H groups of isophthalates, prevent coplanarity of the isophthalates in the structures reported herein.

Owing to the significant repulsions in BADI<sup>4-</sup>, rather than behaving as a 4-connected rectangular-planar node, it adopts the geometry of a pseudo-tetrahedral node. When considering the metal SBU as a 4-connected square planar node and BADI<sup>4-</sup> as a 4-connected pseudo-tetrahedral node, **1-S** may be described as a 4,4-connected network with 4<sup>2</sup>·8<sup>4</sup> topology (**pts** net).<sup>16</sup> Though **1-S** exhibits structural similarities to NOTT-109 (2-D Cu-isophthalate layers), NOTT-109 forms an **ssb** net when treating metal and ligand SBUs in a comparable manner. In some previous reports, tetracarboxylate ligands comparable to H<sub>4</sub>BADI have been treated as two 3-connected nodes by considering the isophthalates as building units extending from the 1,3, and 5 positions. In treating the ligand as such, and maintaining the Cu<sub>2</sub>-paddlewheel as a 4-connected node, **nbo**-type MOFs such as NOTT-102, ZJU-105, Cu<sub>2</sub>ADEDA, and PCN-14 (among others) may be described as having **fov** net topology, and NOTT-109 as **stx** net. **1-S**, however, may be described as having **sur** net topology when treating the ligand and metal SBUs in the same manner.<sup>17</sup>

Stemming from this observation, we searched the literature for other **pts**-type MOFs built from tetracarboxylate ligands without definitive tetrahedral center (termed “non-regular tetrahedral” nodes<sup>18</sup>). Treating the ligand ABTC<sup>4-</sup> (3,3',5,5'-azobenzenetetracarboxylate) as two 3-connected nodes and the metal SBUs as 4-connected nodes, JUC-63<sup>19</sup> and Cd<sub>2</sub>ABTC<sup>20</sup> may be described as having **tfi** net topology, and JUC-64<sup>19</sup> as **dmd** net. Mn<sub>2</sub>TADIP<sup>21</sup> (TADIP<sup>4-</sup> = 5,5'-(1H-1,2,3-triazole-1,4-diyl)diisophthalate) also produces a **tfi** net when considering the ligand TADIP<sup>4-</sup> as two 3-connected nodes and Mn<sub>2</sub>-SBU as a 4-connected node. However, similar treatment of PCN-38 and PCN-39,<sup>22</sup> and both isomers of Cu<sub>2</sub>TCPPDA<sup>23</sup> (TCPPDA = *N,N,N',N'*-tetrakis(4-carboxyphenyl)-1,4-phenylenediamine) results in **sur** net topology.<sup>16</sup> A distinguishing factor that contributes to the differences in topological assessment of this series of MOFs exists in the metal SBU. All the aforementioned MOFs that produce **sur** topology upon treating the ligand as two 3-connected nodes consist of square planar dimetal-paddlewheel SBU, whereas JUC-63, JUC-64, Cd<sub>2</sub>ABTC, and Mn<sub>2</sub>TADIP form distorted tetrahedral metal SBUs.

In addition to the **1-S** MOFs, we synthesized the Zn-based MOF, **2**, which crystallizes in the orthorhombic space group *Fdd2* (#43, parameters:  $a = 38.97$  Å,  $b = 24.82$  Å,  $c = 13.80$  Å) with the asymmetric unit composed of one Zn<sup>2+</sup> cation, half of



a  $\text{BADI}^{4-}$  ligand, and four DMF molecules (two coordinated to the  $\text{Zn}^{2+}$  ion and two solvates). The zinc ion coordinates with two carboxylates on  $\text{BADI}^{4-}$  in an  $\eta^1$ -fashion and two DMF molecules to form a distorted tetrahedral geometry. Each  $\text{BADI}^{4-}$  ligand, therefore, extends the system into 2-D sheets spanning the *ac*-plane, with DMF solvates occupying interlayer spaces. Potential pores are observed along the [011] direction but are filled with coordinated solvent molecules. Since the metal SBU is a single  $\text{Zn}^{2+}$  ion, it is unreasonable to expect these pores to be accessed since the removal of solvent molecules would result in significant destabilization of the framework. As such, no further analysis of 2 was conducted.

### Solvent-responsive phase transformations

We identified that soaking **1-DMA** in DMF (**1-DMA**  $\rightarrow$  DMF) and heating at 85 °C for 18 h results in isolation of **1-DMF** (Fig. 7). This phase change is reversible upon exchanging the solvent with DMA (Fig. S27†), though the solvent exchanges with single-crystals caused the crystal to fracture, preventing the desired single-crystal-to-single-crystal phase transformation. Phase transformation from **1-DMF** to **1-DMA** occurred at room temperature, as well, but the reverse transformation was incomplete after 18 h at room temperature. These preliminary observations led to extensive experimentation of solvent-exchange induced structural transformation in **1-S**. Initial investigation indicated that **1-DMA** and **1-DMF** both converge to the same structure when exchanged with the same solvent. Once we identified the reversible interconversion between **1-DMA** and **1-DMF**, we focused our efforts exclusively on the exchange of a broad range of solvents with **1-DMF**. PXRD results of the range of solvent-induced transformations are shown in Fig. S27–S33.† Herein, we highlight some of the more significant features.

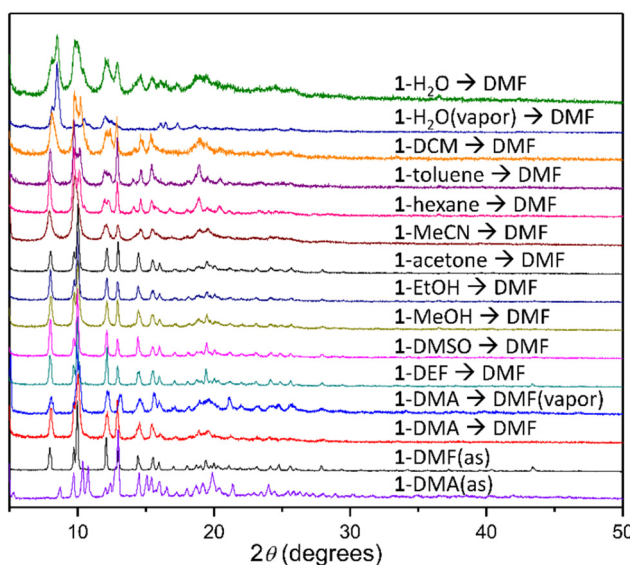


Fig. 7 PXRD patterns of **1-S**  $\rightarrow$  DMF compared to **1-DMF(as)** and **-DMA(as)**.

Exchanging **1-DMF** with DMSO resulted in the isolation of single-crystals suitable for X-ray structural determination, though crystal twinning resulted in an inability to definitively identify solvent molecule positions. Introduction of the non-coordinating solvents toluene and hexane to **1-DMF** results in the MOFs **1-toluene** and **-hexane** exhibiting PXRD patterns closely resembling those of **1-DMA** (Fig. S30†). Soaking **1-DMF** in highly volatile, polar solvents (acetonitrile (MeCN), dichloromethane (DCM), methanol (MeOH), ethanol (EtOH), and acetone) results in loss of crystallinity of the MOF (Fig. S31†). Water-exchange provides PXRD patterns unique from the parent **1-DMF** and **-DMA** and feature significantly broadened signals indicative of loss of crystallinity.

The crystallinity of **1-DMF**  $\rightarrow$   $S_{\text{volatile}}$  ( $S_{\text{volatile}} = \text{MeCN}$ , MeOH, EtOH, DCM, acetone) decreased most significantly upon drying in air, as evidenced from PXRD experiments (Fig. S31†). Additionally, crystals of **1-DMF**  $\rightarrow$  DCM were screened for single-crystal XRD, giving unit cell parameters equivalent to **1-DMF**, though diffuse scattering and cracking of the crystals was observed. Cracking became more pronounced the longer the sample was removed from the solvent, which caused rapid deterioration of crystallinity as the solvent evaporated. Near-complete loss of crystallinity occurred after approximately 1 h under ambient conditions.

After exploring solvent exchange of **1-DMF** with a variety of solvents, we explored the reversibility of this solvent exchange process; most of the crystalline phases reversibly transformed back to **1-DMF**, including **1-DMA**, **-DEF**, **-DMSO**, **-MeOH**, **-EtOH**, and **-acetone** (Fig. 7). In addition, **1-MeCN**  $\rightarrow$  DMF results in slight broadening of peaks in the PXRD diffractogram, indicating imperfect conversion. **1-Hexane**  $\rightarrow$  DMF and **-toluene**  $\rightarrow$  DMF exhibit unique PXRD patterns resembling **1-DMF**, but with notable discrepancies. In particular, the PXRD patterns of these two materials show an inversion of the relative intensities of the peaks centered around  $2\theta$  of 10°, splitting of the peak at 12° into two separate signals, and additional variations at a higher angle. The PXRD pattern for **1-DCM**  $\rightarrow$  DMF also closely resembles the patterns for **1-hexane**  $\rightarrow$  DMF and **-toluene**  $\rightarrow$  DMF. Furthermore, a similar PXRD pattern is observed for **1-H<sub>2</sub>O**  $\rightarrow$  DMF, though signals are broadened to an even greater extent. Most likely, this indicates partial reclamation of the initial **1-DMF** structure, along with increased disorder due to strongly coordinated water molecules or the presence of larger solvent molecules which impede complete structural transformation. To prove that **1-DMF** is reproduced *via* solvent-induced structural transformation rather than a resynthesis pathway, **1-acetone**  $\rightarrow$  DMF was stored at room temperature for 24 h, rather than heating at 85 °C. The collected PXRD pattern of **1-acetone**  $\rightarrow$  DMF matches that of **1-DMF**.

The ability of a seemingly rigid MOF to transition to an amorphous, or nearly amorphous, phase without loss of framework connectivity, and reclamation of crystallinity upon external stimuli is a largely unstudied phenomenon. Currently, the only process described to contribute to such behavior in MOFs has been termed “frustrated flexibility”.<sup>9</sup> Since the



genesis of frustrated flexibility has been attributed to “an incompatibility of intra-framework dispersion forces with the geometrical constraints of the inorganic building units”, we hypothesize that the anthracenyl moieties in **1-S** can result in such dispersion forces leading to a disordered MOF upon removal of solvent molecules coordinated to the terminal positions of the dicopper-paddlewheel SBU. The presence of DMA, DMF, DEF, or DMSO on those terminal coordination sites results in additional dispersion forces that stabilize the crystalline structures. While sophisticated computational and experimental analyses could more definitively evaluate this hypothesis by investigating local-structural changes, we do not currently have the resources to conduct those experiments. Nonetheless, such crystalline-amorphous-crystalline solvent-induced transformations remain rare in MOFs, and it stands to reason that the close proximity of neighboring anthracenyl moieties and significant distortions in copper-paddlewheel SBUs lend credence to this hypothesis.

### MOF activation and gas sorption analyses

Initial attempts to activate **1-S** involved the exchange of mother liquor with the fresh solvent used during the synthesis (3×), followed by the exchange with methanol (3×) and dichloromethane (3×). The solvent-exchanged samples were then heated at 100 °C under dynamic vacuum for 12 h and then further activated using the outgas program on an ASAP 2020 Plus at 30 °C for 24 h. PXRD patterns for activated **1-S** (termed **1-ac**) and **1-ac** → DMF are included in Fig. S33.† Initial N<sub>2</sub> and CO<sub>2</sub> sorption measurements on **1-DMF** and -DMA treated in such a fashion resulted in minimal uptake (Fig. S35†). Attempts were also made to use the freeze-drying method to activate **1-DMF** prior to N<sub>2</sub> sorption measurement; however, no significant improvement in uptake was observed.

## Conclusions

We have successfully solvothermally synthesized a series of copper-based MOFs (**1-S**, *S* = DMF, DEF, DMA) incorporating a bulky, highly aromatic tetracarboxylate ligand and possessing a **pts** net topology exhibiting solvent-induced structural transformations, yielding **1-S**<sub>2</sub> (*S*<sub>2</sub> = DMF, DEF, DMA, DMSO, EtOH, MeOH, MeCN, DCM, acetone, hexane, toluene, H<sub>2</sub>O). Exchanging the solvent of **1-S** with highly volatile solvents (EtOH, MeOH, MeCN, DCM, and acetone) results in significant loss of crystallinity which can be reobtained upon exposure to DMF, indicating that **1-S** likely exhibits “frustrated flexibility”. In fact, the majority of solvent-induced structural transformations reversibly convert back into **1-DMF** upon heating in DMF. Three unique crystal structures are reported from single-crystal X-ray diffraction experiments, including one obtained from a single-crystal-to-single-crystal transformation. Owing to steric hindrance, carboxylates and dicopper paddlewheels in the framework are distorted upon the exchange of terminally coordinated guest molecules. The structural features are com-

pared to those of several other copper-based tetracarboxylate MOFs, particularly MOFs with **nbo** and **pts** net topologies.

We are currently investigating the application of **1-S** in organic dye removal from aqueous solutions and additional methods to produce **nbo**-type MOFs with bulky, highly aromatic tetracarboxylate ligands to better understand the role of highly aromatic groups in various applications. Thorough investigation of local-structural changes in **1-S** upon solvent exchange would provide further insights into the concept of frustrated flexibility in MOFs produced from ligands with no flexible pendant groups.

## Experimental section

### General information

All initial reagents were purchased from commercial sources and used as received without further purification. Nuclear magnetic resonance (NMR) data were collected on a 400 MHz Bruker AVANCE III HD spectrometer. Powder X-ray diffraction (PXRD) patterns were collected on a Bruker D2 Phaser equipped with a copper anode ( $K_{\alpha} = 1.54056 \text{ \AA}$ ),  $K_{\beta}$ -filter, and LYNXEYE 1D silicon strip detector, and operated at 30 kV and 10 mA. Samples analyzed *via* PXRD were dispersed on a Si single-crystal low-background diffraction plate or a back-loading sample holder for analysis. Simulation of PXRD patterns was carried out by using the single-crystal data and diffraction-crystal module of the Mercury program available free-of-charge at <https://www.ccdc.cam.ac.uk/solutions/software/mercury>.<sup>15</sup> Single-crystal XRD data were collected on a Rigaku Oxford Diffraction Synergy-S diffractometer equipped with a HyPix6000HE detector operating with either CuK $\alpha$  or MoK $\alpha$  radiation. The data collection routine, unit cell refinement, and data processing were carried out with the program CrysAlisPro,<sup>24</sup> and structures solved using SHELXT<sup>25</sup> and refined using SHELXL<sup>26</sup> *via* Olex2.<sup>27</sup> Thermogravimetric analyses were performed under nitrogen flow from 50 to 650 °C on a PerkinElmer TGA 4000 analyser with a heating rate of 10 °C min<sup>-1</sup>. Infrared spectra were collected on a PerkinElmer Spectrum 100 FT-IR spectrometer equipped with an attenuated total reflectance accessory. N<sub>2</sub> and CO<sub>2</sub> gas sorption analyses were conducted using Micromeritics ASAP 2020 Plus analyser at 77 K for N<sub>2</sub> and at 273 K and 298 K for CO<sub>2</sub>.

### Synthesis of tetramethyl 5,5'-([9,9'-bianthracene]-10,10'-diyl) diisophthalate (Me<sub>4</sub>BADI)

Me<sub>4</sub>BADI was synthesized *via* the Suzuki–Miyaura cross-coupling reaction in which 10,10'-dibromo-9,9'-bianthryl (1.998 g, 3.901 mmol) was combined with 3,5-bis(methoxycarbonyl) phenylboronic acid (3.718 g, 13.35 mmol), tetrakis(triphenylphosphine)palladium(0) (0.68 g, 0.59 mmol) and potassium carbonate (1.70 g, 12.3 mmol) in a 100 mL Schlenk flask equipped with a Teflon-coated magnetic stir bar. The flask was purged and backfilled with argon three times. A mixture of toluene (15 mL), ethanol (10 mL), and water (5 mL) was bubbled with argon and added to the reaction flask using a



cannula. The rubber septum was replaced with a reflux condenser, and the reaction mixture was heated at reflux under argon with stirring for six days. The organic solvent was then removed using a rotary evaporator, and the aqueous phase was extracted with chloroform, dried over magnesium sulfate, filtered, and reduced *in vacuo*. The resultant solid was washed with acetone until the washings were colorless, yielding a light-yellow solid that was subsequently dried in air (2.497 g, 87% yield). Found: C, 78.98; H, 4.89. Calc. for  $C_{48}H_{34}O_8$ : C, 78.04; H, 4.64%.  $^1H$  NMR (400 MHz,  $CDCl_3$ ):  $\delta$  (ppm) 8.97 (t, 2H,  $J$  = 1.6 Hz), 8.53 (d, 4H,  $J$  = 1.6 Hz), 7.67 (m, 4H), 7.37 (m, 4H), 7.27 (m, 4H), 7.24 (m, 4H), 4.01 (s, 12H).  $^{13}C$  NMR (100 MHz,  $CDCl_3$ ):  $\delta$  (ppm) 166.25, 140.00, 136.72, 135.27, 134.14, 131.28, 131.21, 130.18, 129.97, 127.22, 126.53, 125.93, 125.84, 52.55.

### Synthesis of 5,5'-(9,9'-bianthracene)-10,10'-diyl)diisophthalic acid ( $H_4BADI$ )

$Me_4BADI$  (2.497 g, 3.380 mmol) was combined with potassium hydroxide (1.6 g) in a mixture of water and tetrahydrofuran (THF, 40 mL, 1:1 by volume) and heated at reflux for 24 hours. The mixture was then cooled and filtered to remove the black precipitate before THF was removed *in vacuo*. The remaining aqueous mixture was acidified with 10% aqueous hydrochloric acid until a yellow precipitate was observed. The precipitate was collected *via* vacuum filtration, washed with water, and dried at 110 °C in air (yield: 2.286 g, 99%). Found: C, 76.37; H, 4.06. Calc. for  $C_{44}H_{26}O_8$ : C, 77.41; H, 3.84%.  $^1H$  NMR (400 MHz,  $DMSO-d_6$ ):  $\delta$  (ppm) 13.50 (s, 4H), 8.76 (t, 2H,  $J$  = 1.6 Hz), 8.38 (d, 4H,  $J$  = 1.6 Hz), 7.65 (d, 4H,  $J$  = 8.8 Hz), 7.47 (m, 4H), 7.28 (m, 4H), 7.15 (d, 4H,  $J$  = 8.8 Hz).  $^{13}C$  NMR (100 MHz,  $DMSO-d_6$ ):  $\delta$  (ppm) 166.60, 139.02, 135.70, 135.36, 133.35, 132.19, 130.68, 129.55, 129.43, 126.68, 126.33, 126.27, 126.21.

### Synthesis of $Cu_2BADI(DMA)_x(H_2O)_y$ ( $Cu_2BADI-DMA$ , 1-DMA)

To a 20 mL scintillation vial was added  $H_4BADI$  (0.050 g, 0.073 mmol),  $Cu(NO_3)_2 \cdot 2.5H_2O$  (0.050 g, 0.21 mmol), and *N,N*-dimethylacetamide (DMA, 15 mL), followed by addition of  $HBF_4$  (1000  $\mu$ L). The vial was sealed with a Teflon-lined plastic screw cap and heated at 85 °C in an oven for 48 hours. The resultant green crystalline material named  $Cu_2BADI-DMA$  (1-DMA) was decanted and washed with fresh DMA. Yield: 54 mg.

### Synthesis of $Cu_2BADI(DMF)_x(H_2O)_y$ ( $Cu_2BADI-DMF$ , 1-DMF)

To a 20 mL scintillation vial was added  $H_4BADI$  (0.050 g, 0.073 mmol),  $Cu(NO_3)_2 \cdot 2.5H_2O$  (0.050 g, 0.21 mmol), and *N,N*-dimethylformamide (DMF, 15 mL), followed by addition of  $HBF_4$  (1000  $\mu$ L). The vial was heated (uncapped) at 85 °C in an oven for 48 hours. The resultant green crystalline material named  $Cu_2BADI-DMF$  (1-DMF) was decanted and washed with fresh DMF. Yield: 81 mg.

The MOF 1-DMF was also isolable from a 5× scaled-up reaction in which 250 mg of  $H_4BADI$  was combined with 250 mg of  $Cu(NO_3)_2 \cdot 2.5H_2O$  in 75 mL of DMF and 2.50 mL of  $HBF_4$  in a 150 mL beaker, and heated (uncovered) in an oven at 85 °C for

48 hours. The crystalline solid was decanted and washed with fresh DMF. Yield: 471 mg.

### Synthesis of $Cu_2BADI(DEF)_x(H_2O)_y$ ( $Cu_2BADI-DEF$ , 1-DEF)

To a 20 mL scintillation vial was added  $H_4BADI$  (0.050 g, 0.073 mmol),  $Cu(NO_3)_2 \cdot 2.5H_2O$  (0.050 g, 0.21 mmol), and *N,N*-diethylformamide (DEF, 15 mL), followed by addition of  $HBF_4$  (500  $\mu$ L). The vial was heated (uncapped) at 85 °C in an oven for 48 hours. The resultant green crystalline material named  $Cu_2BADI-DEF$  (1-DEF) was decanted and washed with fresh DEF. Yield: 31 mg.

### Synthesis of $Zn_2BADI-S$ ( $S$ = unidentified solvent) (2)

To a 1-dram vial was added  $H_4BADI$  (0.005 g, 0.0073 mmol),  $Zn(NO_3)_2 \cdot 6H_2O$  (0.005 g, 0.017 mmol), and DMF (1.5 mL), followed by addition of  $HBF_4$  (100  $\mu$ L). The vial was sealed with a plastic screw cap and heated at 85 °C in an oven for 48 hours. The resultant yellowish crystalline material named  $Zn_2BADI$  was decanted and washed with fresh DMF. Individual crystals suitable for evaluation *via* single-crystal X-ray diffraction were isolated from the mixture. Yield was not determined and conditions were not refined, as the determined structure was not of significant interest.

### Solvent exchange experiments

To a 20 mL scintillation vial was added 20–50 mg of 1- $S_1$  that had been previously dried in air, followed by addition of ~20 mL of exchange-solvent ( $S_2$ ) and the vial capped with a Teflon-lined plastic screw cap. For solvents with boiling points greater than 85 °C, the sample was then heated at 85 °C in an oven for 24 h. For solvents with boiling points less than 85 °C, the sample was stored at room temperature for 24 h. Samples of 1- $S_1 \rightarrow S_2$  were then isolated by collecting the solid on filter paper and drying at room temperature. Dry samples were characterized *via* PXRD. The sample 1-acetone  $\rightarrow$  DMF was stored at room temperature for 24 h to show that the reproduction of 1-DMF is truly a solvent-induced structural transformation rather than a resynthesis pathway.

Vapor diffusion experiments were conducted by transferring 10–20 mg of 1- $S_1$  to a 1-dram vial which was then nestled in a 20 mL scintillation vial filled with 5 mL of exchange-solvent ( $S_2$ ). For solvents with boiling points greater than 85 °C, the sample was then heated at 85 °C in an oven for 24 h. For solvents with boiling points less than 85 °C, the sample was stored at room temperature for 24 h. Samples of 1- $S_1 \rightarrow S_2$ (vapor) were then isolated by collecting the solid on filter paper and drying them at room temperature. Dry samples were characterized *via* PXRD.

### Data availability

The data supporting this article have been included as part of the ESI.† CCDC 2324983–2324986 contain the supplementary crystallographic data for this paper.



## Conflicts of interest

There are no conflicts of interest to declare.

## Acknowledgements

TAM, AE, and LJE acknowledge the support of the Van W. Daniel, III Endowed Professorship in Chemistry Fund and the UVA Wise Fellowship in the Natural Sciences. TAM and AE were partially supported by the National Science Foundation under grant number DUE-1833781, and single-crystal crystallography experiments were supported under grant number CHE-1726077. Q. Zhang would like to acknowledge the financial support from the ACS-PRF grant under grant number 60705-DNI10.

## References

- 1 S. R. Batten, N. R. Champness, X.-M. Chen, J. Garcia-Martinez, S. Kitagawa, L. Öhrström, M. O'Keeffe, M. P. Suh and J. Reedijk, *Pure Appl. Chem.*, 2013, **85**, 1715–1724.
- 2 H.-C. Zhou, J. R. Long and O. M. Yaghi, *Chem. Rev.*, 2012, **112**, 673–674.
- 3 R. J. Kuppler, D. J. Timmons, Q.-R. Fang, J.-R. Li, T. A. Makal, M. D. Young, D. Yuan, D. Zhao, W. Zhuang and H.-C. Zhou, *Coord. Chem. Rev.*, 2009, **253**, 3042–3066.
- 4 H. Furukawa, K. E. Cordova, M. O'Keeffe and O. M. Yaghi, *Science*, 2013, **341**, 1230444.
- 5 A. Schneemann, V. Bon, I. Schwedler, I. Senkovska, S. Kaskel and R. A. Fischer, *Chem. Soc. Rev.*, 2014, **43**, 6062–6096.
- 6 Q. Zhang, J. Su, D. Feng, Z. Wei, X. Zou and H.-C. Zhou, *J. Am. Chem. Soc.*, 2015, **137**, 10064–10067.
- 7 I. Senkovska, V. Bon, L. Abylgazina, M. Mendt, J. Berger, G. Kieslich, P. Petkov, J. Luiz Fiorio, J.-O. Joswig, T. Heine, L. Schaper, C. Bachetzky, R. Schmid, R. A. Fischer, A. Pöppl, E. Brunner and S. Kaskel, *Angew. Chem., Int. Ed.*, 2023, **62**, e202218076.
- 8 S. Neogi, S. Sen and P. K. Bharadwaj, in *Encyclopedia of Inorganic and Bioinorganic Chemistry*, ed. R. A. Scott, 2014, pp. 1–50. DOI: [10.1002/9781119951438.eibc2223](https://doi.org/10.1002/9781119951438.eibc2223).
- 9 R. Pallach, J. Keupp, K. Terlinden, L. Frentzel-Beyme, M. Kloß, A. Machalica, J. Kotschy, S. K. Vasa, P. A. Chater, C. Sternemann, M. T. Wharmby, R. Linser, R. Schmid and S. Henke, *Nat. Commun.*, 2021, **12**, 4097.
- 10 C. E. Wilmer, M. Leaf, C. Y. Lee, O. K. Farha, B. G. Hauser, J. T. Hupp and R. Q. Snurr, *Nat. Chem.*, 2012, **4**, 83–89.
- 11 K. Shao, J. Pei, J.-X. Wang, Y. Yang, Y. Cui, W. Zhou, T. Yildirim, B. Li, B. Chen and G. Qian, *Chem. Commun.*, 2019, **55**, 11402–11405.
- 12 X. Lin, I. Telepeni, A. J. Blake, A. Dailly, C. M. Brown, J. M. Simmons, M. Zoppi, G. S. Walker, K. M. Thomas, T. J. Mays, P. Hubberstey, N. R. Champness and M. Schröder, *J. Am. Chem. Soc.*, 2009, **131**, 2159–2171.
- 13 S. Ma, D. Sun, J. M. Simmons, C. D. Collier, D. Yuan and H.-C. Zhou, *J. Am. Chem. Soc.*, 2008, **130**, 1012–1016.
- 14 J. Zhao, R. Lin, W. Tian, X. Zhu, X. Luo and Y. Liu, *Cryst. Growth Des.*, 2023, **23**, 4417–4423.
- 15 C. F. Macrae, I. Sovago, S. J. Cottrell, P. T. A. Galek, P. McCabe, E. Pidcock, M. Platings, G. P. Shields, J. S. Stevens, M. Towler and P. A. Wood, *J. Appl. Crystallogr.*, 2020, **53**, 226–235.
- 16 V. A. Blatov, A. P. Shevchenko and D. M. Proserpio, *Cryst. Growth Des.*, 2014, **14**, 3576–3586.
- 17 A. P. Shevchenko, A. A. Shabalin, I. Y. Karpukhin and V. A. Blatov, *Sci. Technol. Adv. Mater.: Methods*, 2022, **2**, 250–265.
- 18 W. Lu, Z. Wei, Z.-Y. Gu, T.-F. Liu, J. Park, J. Park, J. Tian, M. Zhang, Q. Zhang, T. Gentle Iii, M. Bosch and H.-C. Zhou, *Chem. Soc. Rev.*, 2014, **43**, 5561–5593.
- 19 M. Xue, G. Zhu, Y. Li, X. Zhao, Z. Jin, E. Kang and S. Qiu, *Cryst. Growth Des.*, 2008, **8**, 2478–2483.
- 20 Q.-F. Zhang, J.-H. Luo and A.-H. Yuan, *Z. Anorg. Allg. Chem.*, 2013, **639**, 1804–1807.
- 21 L. Sun, Q. Pan, Z. Liang and J. Yu, *Inorg. Chem. Front.*, 2014, **1**, 478–486.
- 22 T. A. Makal, W. Zhuang and H.-C. Zhou, *J. Mater. Chem. A*, 2013, **1**, 13502–13509.
- 23 D. Sun, Y. Ke, T. M. Mattox, B. A. Ooro and H.-C. Zhou, *Chem. Commun.*, 2005, 5447–5449.
- 24 *CrysAlisPro Software System, v1.171.42.xx, R. O. Diffraction*, Rigaku Corporation, Oxford, UK, 2022.
- 25 G. M. Sheldrick, *Acta Crystallogr., Sect. A: Found. Adv.*, 2015, **71**, 3–8.
- 26 G. M. Sheldrick, *Acta Crystallogr., Sect. C: Struct. Chem.*, 2015, **71**, 3–8.
- 27 O. V. Dolomanov, L. J. Bourhis, R. J. Gildea, J. A. K. Howard and H. Puschmann, *J. Appl. Crystallogr.*, 2009, **42**, 339–341.

